Geophys. J. R. astr. Soc. (1982) **70**, 399–414

Lithosphere response to externally and internally derived stresses: a viscoelastic stress guide with amplification

N. J. Kusznir *Department of Geology, University of Keele, Keele, Staffs ST5 5BG*

Received 1981 December 23; in original form 1981 July 20

Summary. Lithosphere subjected to an externally derived horizontal stress undergoes creep in the lower lithosphere resulting in the decay of lower lithosphere stress and the associated amplification of stress within the upper lithosphere. This stress response of lithosphere has been investigated for a lithosphere model with power-law stress and temperature dependent viscoelastic properties. The rate and extent of stress decay and associated stress amplification is greatly dependent on the lithosphere geotherm.

Oceanic lithosphere subject to an applied stress of ± 0.1 kb undergoes upper lithosphere stress amplification of × 1.5, × 1.8 and × 2.0 at 10^4, 10^6 and 10^8 yr respectively. At 10^6 yr the effective lithosphere thickness is reduced to approximately 40 km. The stress decay and amplification proceeds more rapidly for an applied stress of ± 1.0 kb and in the case of a tensile applied stress results in some upper lithosphere fracture. For continental and Basin and Range type lithosphere the comparable stress amplification at 10^6 yr, for a stress of ± 0.1 kb, is × 2.0 and × 6.5 with effective lithosphere thicknesses of 60 and 20 km respectively. The large values of stress amplification for the Basin and Range lithosphere result in complete upper lithosphere fracture which gives rise to a cyclic process of upper lithosphere faulting and lower lithosphere creep in which extensive lithosphere deformation can occur.

The stress amplification process also occurs for stresses generated by lateral density contrasts. For an isostatically compensated plateau uplift structure, deviatoric stresses of the order of 1 kb can be generated in the upper lithosphere by this process and are sufficient to cause tensile fracture of the upper lithosphere. The response of viscoelastic lithosphere to constant geometry bending stresses has also been examined and results in substantial but not complete reduction of the bending stresses.

1 Introduction

The concept of a strong and rigid lithosphere overlying the weaker semifluid asthenosphere is central to the plate tectonics hypothesis. The thickness of the lithosphere may be defined by seismic experiment, by thermal consideration and by flexural rigidity studies. The lithosphere acts as a stress guide because its mechanical structure allows it to sustain static

stresses while the asthenosphere is incapable of doing so. Some compositional difference may exist between lithosphere and asthenosphere; however, the differences between the generally brittle and elastic properties of the lithosphere and the semifluid-non-elastic properties of the asthenosphere arises due to the different relationship between the geotherm and the melting temperature for each body. While the relative coolness of the lithosphere with respect to its melting temperature defines its largely elastic properties, the partially molten state of the asthenosphere defines its viscous non-elastic properties. The boundary between lithosphere and asthenosphere may be defined by a temperature with respect to the melting point which distinguishes between material which behaves elastically and that which behaves non-elastically. Such a definition results in a gradual transition from lithosphere to asthenosphere with increasing depth. Within this transitional zone the observed response of material in terms of elastic or viscous/non-elastic behaviour will be dependent on the time period over which the behaviour is examined. Consequently, the depth to the lithosphere–asthenosphere transition is time dependent and assessments of lithosphere thickness by lithosphere response to different mechanical stimuli of different ages will result in different thicknesses.

Lithosphere thickness estimates from lithosphere flexure response to glacial unloading consider mechanical behaviour over time periods of the order of 10 000 yr and suggest lithosphere thicknesses of the order of 100 km or so (Haskell 1937; Cathles 1975). Walcott (1970) has shown that the effective lithosphere rigidity and thickness decrease with time. Walcott suggested that the lithosphere may be regarded as a composite elastic/viscoelastic plate in which the upper $^1/_5$ behaves elastically while the lower $^4/_5$ behaves viscoelastically with an effective viscosity of 10^{23} Pa s. Determination of lithosphere thickness by seismology, a technique which examines lithosphere mechanical response over very short time periods, produces lithosphere thickness, as expected, more closely in agreement with those from post-glacial rebound studies.

Watts & Cochran (1974) and Watts, Cochran & Selzer (1975) have examined the lithosphere flexure associated with seamount loads on thermally equilibrated ocean basin and have shown that the effective flexural rigidity reaches a constant and finite value after a few million years from the point of load imposition and they suggested that the lithosphere is then capable of rigidly supporting the load over periods of tens of millions of years. Watts *et al.* (1980) and Casenave *et al.* (1980) have also shown that the oceanic lithosphere thickness deduced from flexural rigidity studies for seamount loads is dependent on the age of the lithosphere at the time of loading and does not depend appreciably on the age of the lithosphere. They have shown that the lithosphere thickness increases with the square root of the lithosphere age at loading and reaches a thickness of about 20–30 km at about 80 Myr. These flexural rigidity estimates are considerably less than the estimates based on thermal models (Forsyth 1977) and seismology (Forsyth 1975). However, the estimates are consistent with the thermal model if the 450°C isotherm is used to define the base of the lithosphere. Casenave *et al.* confirm the suggestion by Watts *et al.* that the stabilization of the flexure associated with the seamount load occurs relatively rapidly compared with the age of the lithosphere and suggest that this stabilization time is at most 6 per cent of the age of the lithosphere at the time of loading.

Kusznir & Bott (1977) and Bott & Kusznir (1979) have examined the behaviour of stress within a composite elastic/viscoelastic lithosphere as suggested by Walcott and have shown that, for externally derived stresses, the decrease in the effective lithosphere thickness with time results in the amplification of applied stresses in the upper elastic part of the lithosphere and decay in the lower non-elastic lithosphere. Kusznir & Bott used for the lower lithosphere a Maxwell viscoelastic rheology with Newtonian viscosity. Laboratory work has shown that

for mantle type rocks the apparent viscosity is non-Newtonian and depends both on temperature and the power of shear stress. Such a viscosity relationship for the lithosphere results in a continuous decrease in viscosity with increase in temperature. While the upper lithosphere has effectively an infinite viscosity and is elastic, the lower lithosphere has viscosities which decrease with depth (Murrell 1976). In this paper the lithosphere response to externally and internally derived stresses is examined for lithosphere with power-law stress-dependent viscoelastic properties.

2 The lithosphere model

Lithosphere material may be modelled most simply as a viscoelastic or plastic body. Since the apparent viscosity or onset of plastic deformation of material depends on temperature, the depth variation of lithosphere mechanical properties will be predominantly controlled by the geotherm. Compositional differences, either laterally or with depth, may further influence mechanical behaviour; however, temperature is expected to be the dominant factor. The lithosphere has been modelled as a viscoelastic material with effective viscosity, η, dependent on the power of deviatoric stress, τ, temperature, T and melting temperature, M such that

$$\eta = A \cdot \exp(BM/T) \cdot \tau^{-n} . \tag{1}$$

The numerical values of the constants A, B and n have been estimated by Neugebauer & Breitmayer (1975) and Woodward (1976) from experimental studies on olivine by Kohlstedt & Goetze (1974) for steady state creep. Equation (1) then becomes

$$\begin{aligned} \eta &= 2.1 \times 10^{14} \exp(40M/T)\tau^{-2}, \quad \tau \leqslant 10^8 \\ \eta &= 1.0 \times 10^{31} \exp(40M/T)\tau^{-4}, \quad \tau \geqslant 10^8 \end{aligned} \tag{2}$$

where τ is in pascals and M and T are in K. The units of η are consequently Pa s.

The above equation describes the apparent viscosity for powerlaw creep (dislocation creep). Goetze (1978) has suggested that the Dorn law may fit the experimental data for olivine for stresses greater than 2 kb. Goetze has also suggested that Coble creep (diffusion creep) may also be significant for large stresses. In this paper power-law creep only has been used. Should, however, the Dorn law be applicable, its effect would be to broaden the transition zone between the elastic upper lithosphere and the inelastic lower lithosphere (Lago & Cazenave 1981).

In this study the mechanical stress response of three types of lithosphere have been examined: oceanic, continental and Basin and Range type continental lithosphere. The fundamental mechanical distinction between these three types of lithosphere arises predominantly due to their different geotherms. Oceanic geotherms have been calculated by many workers using many different techniques and models, e.g. Sclater & Francheteau (1970), Haigh (1973), Mercier & Carter (1975), Schubert, Froidevaux & Yuen (1976) and Forsyth (1977). An ocean basin geotherm based on Haigh (1973) has been used for the oceanic lithosphere model. Similarly for continental lithosphere many different geotherm estimates exist, e.g. Herrin (1972), Mercier & Carter (1975) and Froidevaux & Schubert (1975). The geotherm chosen for continental type lithosphere is that suggested by Herrin for the Canadian shield. The Basin and Range type continental lithosphere geotherm chosen is that suggested by Herrin. The respective geotherms are shown in Figs 2, 4 and 6. The melting temperature/depth relationship is also shown in Figs 2, 4 and 6 and is taken from Green (1973).

In the lithosphere models of this paper the lithosphere thickness need not be explicitly input, since the rapid decrease in viscosity corresponding to the lithosphere/asthenosphere boundary follows from the geotherm and the rheology law of equation (1). However, for the

purpose of comparison and model initiation, the models have been given an initial thickness based on seismic and thermal model estimates of lithosphere thickness.

3 Origins of stress applied to lithosphere models

Turcotte & Oxburgh (1976) have discussed in detail the origins of stress existing within the lithosphere. The sources of stress may be summarized as follows:

(1) lateral density contrasts (e.g. passive continental margins or subduction zones);
(2) thermal stresses (e.g. cooling stress within oceanic lithosphere);
(3) asthenosphere flow drag on lithosphere;
(4) lithosphere bending and flexure;
(5) membrane stresses.

The response of lithosphere to thermal stresses is not described in this paper. For the purposes of this study stresses are categorized into three groups.

(a) Externally derived stresses. These are stresses which are not derived within the piece of lithosphere under consideration but are stress guided to the lithosphere section under consideration from a stress source in adjacent lithosphere. The origins of such stress may be lateral density contrasts (e.g. continental margins or ocean ridges) or asthenosphere drag.

(b) Internally derived stresses. These are stresses which are generated within the section of lithosphere under consideration. In the case studied they are generated by lateral density contrasts.

(c) Stresses arising from lithosphere bending and flexure.

4 The mathematical formulation of the lithosphere stress response to externally derived stress

The lithosphere model is shown in Fig. 1. Externally derived stress, σ_0, is applied in the x-direction to the lithosphere at each end of the model. The piece of lithosphere being examined is assumed to be laterally extensive compared with its thickness.

Conservation of horizontal force enables us to introduce the following equation

$$\int_0^L \sigma_x \, dz = \text{constant} \tag{3}$$

where L is lithosphere thickness. On differentiation with respect to time this becomes

$$\int_0^L \dot{\sigma}_x \, dz = 0. \tag{4}$$

Assuming that the different layers of the lithosphere with differing viscosities are welded together we may write

$$\frac{d\dot{\epsilon}_x}{dz} = 0. \tag{5}$$

This assumption is in any case valid at the lateral centre of the lithosphere model.

Additionally we may assume that plane strain exists in the y-direction, i.e. $\epsilon_y = 0$. Also since the upper surface of the lithosphere is free, for the stress fields arising from the externally applied stress field σ_0, it may be assumed that $\sigma_z = 0$.

The equations for strains ϵ_x, ϵ_y and ϵ_z for a Maxwell viscoelastic material may be written

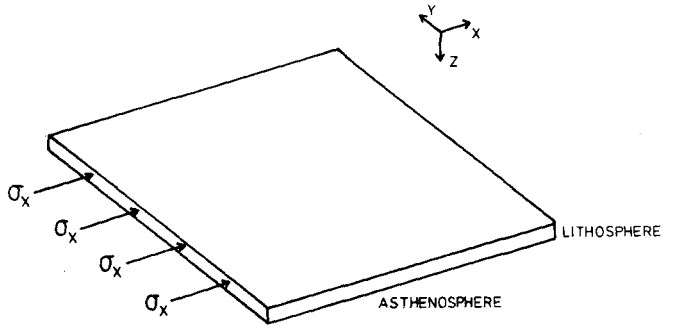

Figure 1. Lithosphere model showing coordinate scheme.

as

$$\epsilon_x = \frac{1}{E}(\sigma_x - \sigma_x^0) - \frac{\nu}{E}(\sigma_y - \sigma_y^0) - \frac{\nu}{E}(\sigma_z - \sigma_z^0) + \epsilon_x^v$$

$$\epsilon_y = \frac{1}{E}(\sigma_y - \sigma_y^0) - \frac{\nu}{E}(\sigma_x - \sigma_x^0) - \frac{\nu}{E}(\sigma_z - \sigma_z^0) + \epsilon_y^v \tag{6}$$

$$\epsilon_z = \frac{1}{E}(\sigma_z - \sigma_z^0) - \frac{\nu}{E}(\sigma_x - \sigma_x^0) - \frac{\nu}{E}(\sigma_y - \sigma_y^0) + \epsilon_z^v ,$$

where σ_x, σ_x^0 and ϵ_x^v are stress, initial stress and creep strain in the x-direction. E is Young's modulus and ν Poisson's ratio.

Creep strain rate $\dot{\epsilon}_x^v$ is given by

$$\dot{\epsilon}_x^v = \frac{(2\sigma_x - \sigma_y - \sigma_z)}{6\eta} \tag{7}$$

and similarly for $\dot{\epsilon}_y^v$ and $\dot{\epsilon}_z^v$. η is apparent viscosity and is given by equation (2).

Substituting $\sigma_z = 0$ and $\epsilon_y = 0$ into equation (6), differentiating respect to time and rearranging we have

$$\dot{\epsilon}_x = \frac{(1-\nu^2)}{E}(\dot{\sigma}_x - \dot{\sigma}_x^0) + \frac{(2\sigma_x - \sigma_y)}{6\eta} + \nu\frac{(2\sigma_y - \sigma_x)}{6\eta} \tag{8}$$

and

$$\dot{\sigma}_y = \nu(\dot{\sigma}_x - \dot{\sigma}_x^0) - E\frac{(2\sigma_y - \sigma_x)}{6\eta} + \dot{\sigma}_y^0 . \tag{9}$$

Manipulation of equations (4), (5) and (8) gives

$$\dot{\sigma}_x = \frac{1}{L}\int_0^L k\dot{\epsilon}_v dz - k\dot{\epsilon}_v - \frac{1}{L}\int_0^L \dot{\sigma}_x^0 dz + \dot{\sigma}_x^0 \tag{10}$$

where

$$k = E/(1-\nu^2)$$

and

$$\dot{\epsilon}_v = \frac{\sigma_x(2-\nu) - \sigma_y(1-2\nu)}{6\eta} .$$

Integration of (10) and (9) gives σ_x and σ_y.

$$\sigma_x = \int_0^t \left(\frac{1}{L}\int_0^L k\dot{\epsilon}_v dz - k\dot{\epsilon}_v\right) dt' - \frac{1}{L}\int_0^L \sigma_x^0 \cdot dz + \sigma_x^0 \tag{11}$$

$$\sigma_y = \int_0^t \left(\nu\dot{\sigma}_x - E\frac{(2\sigma_y - \sigma_x)}{6\eta}\right) dt' + \sigma_y^0 - \nu\sigma_x^0 . \tag{12}$$

The value of σ_x ($t = 0$) is σ_0.

Solution of these two equations has been carried out by the finite difference method. The solutions have been checked using the finite element method to calculate the time and depth behaviour of stress σ_x and σ_y. The results of the method outlined above and those of the finite element method calculated for the laterally central part of the plate agree perfectly confirming that the above approach is valid. The detailed results of the finite element analysis have been described elsewhere (Kusznir & Bott 1977). The integral method described above (equations 11 and 12) is preferred since it is computationally much more rapid and also allows greater numerical resolution and accuracy in both time and depth than the finite element method.

The stresses calculated by equations (11) and (12), when combined with the lithostatic stress component, have been interpreted in terms of lithosphere fracture by application of the Griffiths theory of brittle failure (Murrell 1958). The Griffiths failure criterion can be expressed in terms of the maximum and minimum principal stresses, the tensile strength of the material, T, the coefficient of friction, μ, and the stress required to close cracks, σ_c. Values of $T = 0.5$ kb (Brace 1961), $\mu = 1.09$ (Murrell 1958) and $\sigma_c = -4.19\,T$ have been used. Stress release associated with fracture of lithosphere can be included in the model by the use of the initial stress parameters, σ_x^0 and σ_y^0 in equations (11) and (12). The fracture test is applied after each increment of the finite difference time iteration of equations (11) and (12). Stresses producing fracture are then returned to the failure envelope and the associated stress drop is incorporated in the initial stress term.

5 Lithosphere response to applied externally derived stress

5.1 OCEANIC LITHOSPHERE RESPONSE

The behaviour of stress σ_x as a function of depth and time after stress application is shown in Fig. 2 for $\sigma_0 = 0.1$ kb. Stress σ_x is shown normalized with respect to σ_0. An initial lithosphere thickness of 80 km has been used. Values for Young's modules and Poisson ratio were 10^{11} Pa and 0.25 respectively. The geotherm and melting temperature depth relationship are also shown.

Stress σ_x in the lower lithosphere can be seen to decay as time progresses with the resulting amplification of upper lithosphere stress. At 10^3 yr after initial stress amplification the stress has almost completely decayed to zero in the bottom ¼ of the lithosphere with an amplification factor of approximately × 1.3 in the upper lithosphere. At 10^6 yr stress relaxation has occurred in the lower part of the lithosphere, such that the effective lithosphere thickness is 40 km, with an accompanying amplification factor of × 1.8 in the upper lithosphere. At 10^8 yr the amplification is approximately × 2.0. The stress behaviour is not dependent on whether σ_0 is negative (i.e. compressive) or positive (i.e. tensional).

The time and depth stress behaviour is shown in Fig. 3 for $\sigma_0 = \pm 1.0$ kb. The stress decay and amplification can be seen to proceed more rapidly than for $\sigma_0 = \pm 0.1$ kb. The amplification process in the upper lithosphere may result in stress levels which cause failure and stress

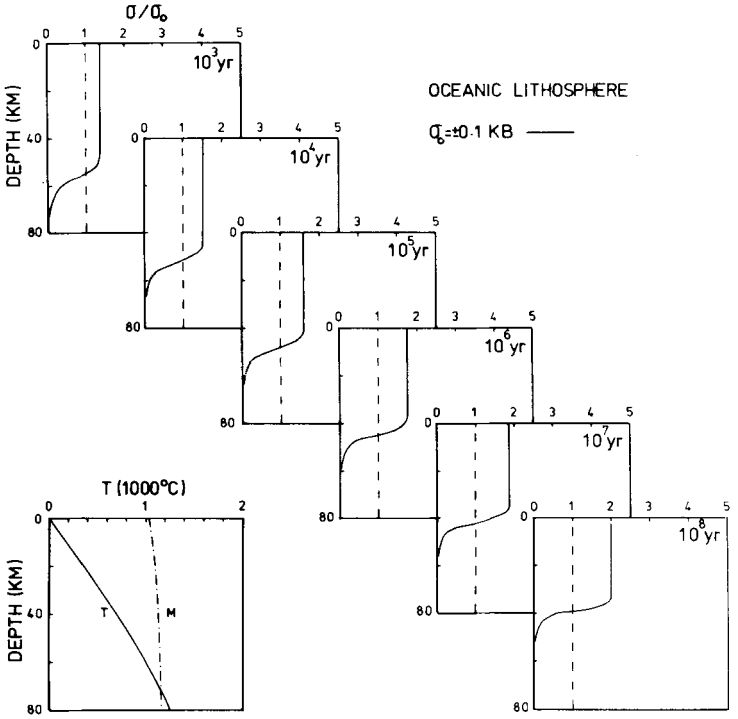

Figure 2. Stress in oceanic lithosphere as a function of depth at various times after initial application of stress. $\sigma_0 = \pm 0.1$ kb.

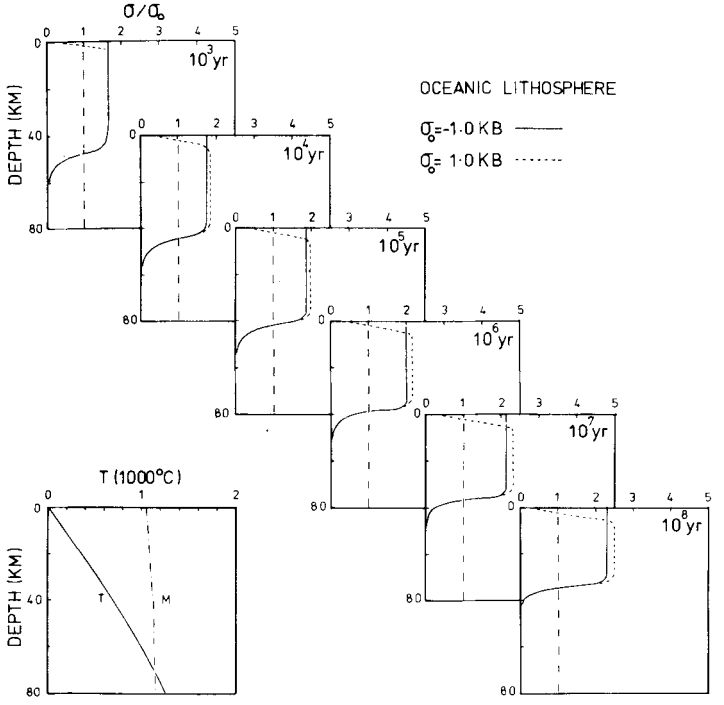

Figure 3. Stress in oceanic lithosphere as a function of depth at various times after initial application of stress. $\sigma_0 = \pm 1.0$ kb.

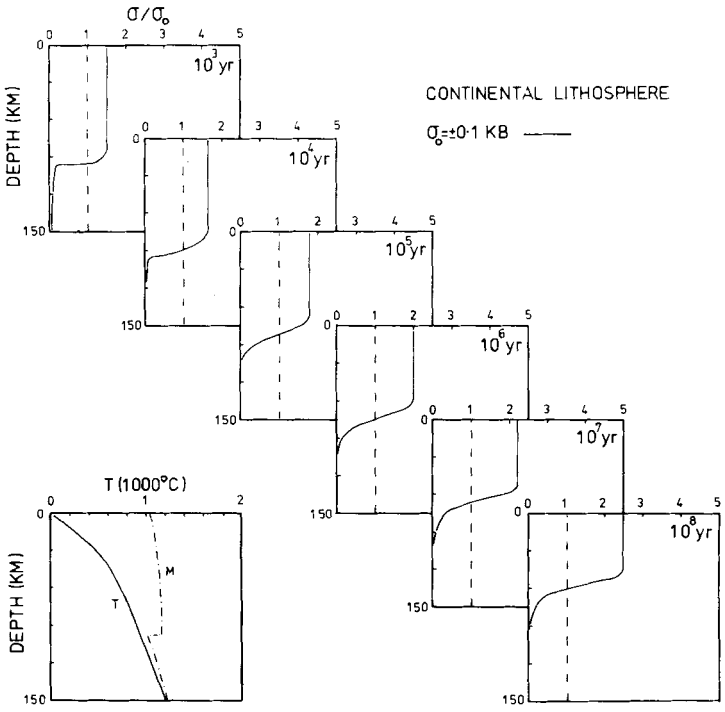

Figure 4. Stress in continental lithosphere as a function of depth at various times after initial application of stress. $\sigma_0 = \pm 0.1$ kb.

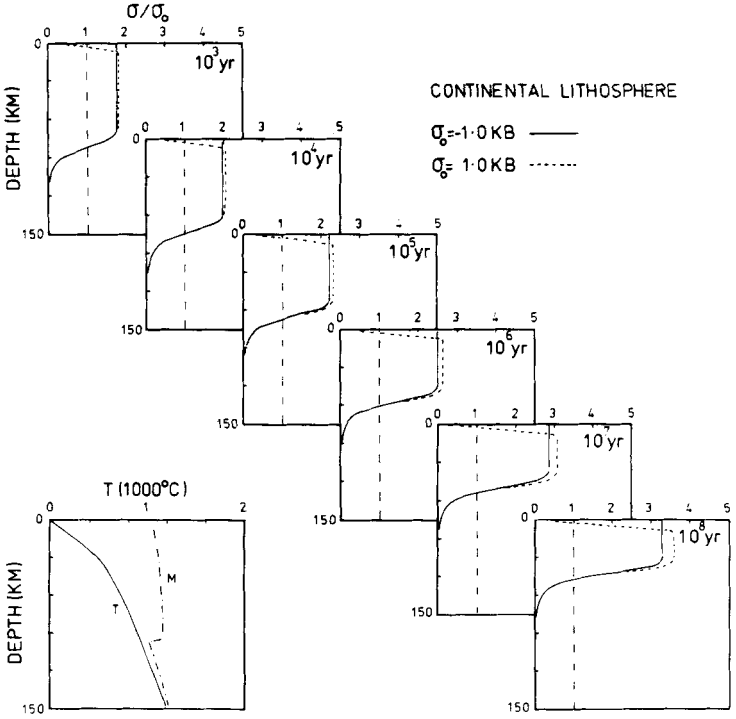

Figure 5. Stress in continental lithosphere as a function of depth at various times after initial application of stress. $\sigma_0 = \pm 1.0$ kb.

release within the upper lithosphere. Failure can be seen to occur for tensional values of σ_0 (positive) but not for compressive values. Failure and stress release in the upper lithosphere result in a further amplification of stress in the lower non-failing elastic lithosphere.

5.2 CONTINENTAL LITHOSPHERE RESPONSE

The response of continental lithosphere to external stress σ_0 is shown in Figs 4 and 5 for values of $\sigma_0 = \pm 0.1$ and ± 1.0 kb respectively. The stress σ_0 has been applied over an initial thickness of 150 km. The geotherm and melting point curve are also shown. Stress decay in the lower lithosphere and associated amplification in the upper lithosphere can be seen again to occur. For an applied stress of ± 0.1 kb stress amplification in the upper lithosphere is $\times 1.6$, $\times 2.0$ and $\times 2.5$ at 10^4, 10^6 and 10^8 yr respectively. The thickness of lithosphere carrying stress at 10^6 yr is about 70 km. Failure again occurs for $\sigma_0 = +1.0$ kb (tensional). Stress decay and amplification proceeds much more rapidly for $\sigma_0 = \pm 1.0$ kb than for ± 0.1 kb.

The decay and amplification of stress appears to be more rapid for continental than oceanic lithosphere. This, however, is partly an artefact arising from the lithosphere thickness value over which the stress σ_0 is initially applied. If an initial thickness for continental lithosphere is used which is comparable with that of the oceanic lithosphere the continental lithosphere then undergoes slower stress transfer resulting in lower amplification factors.

5.3 BASIN AND RANGE TYPE LITHOSPHERE RESPONSE

Stress behaviour with time and depth is shown in Figs 6 and 7 for Basin and Range type lithosphere. Geotherm and melting point curves are again shown. The high goethermal

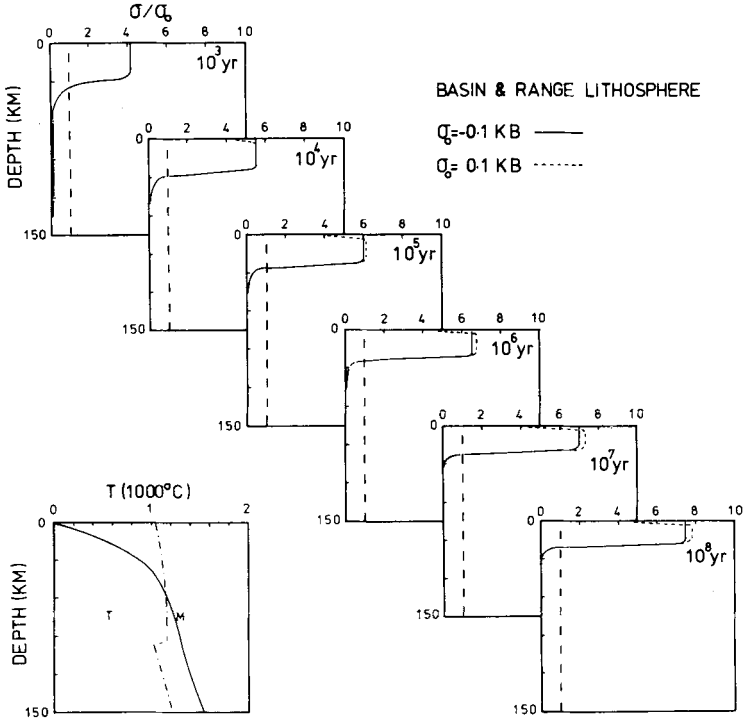

Figure 6. Stress in Basin and Range type lithosphere as a function of depth at various times after initial application of stress. $\sigma_0 = \pm 0.1$ kb.

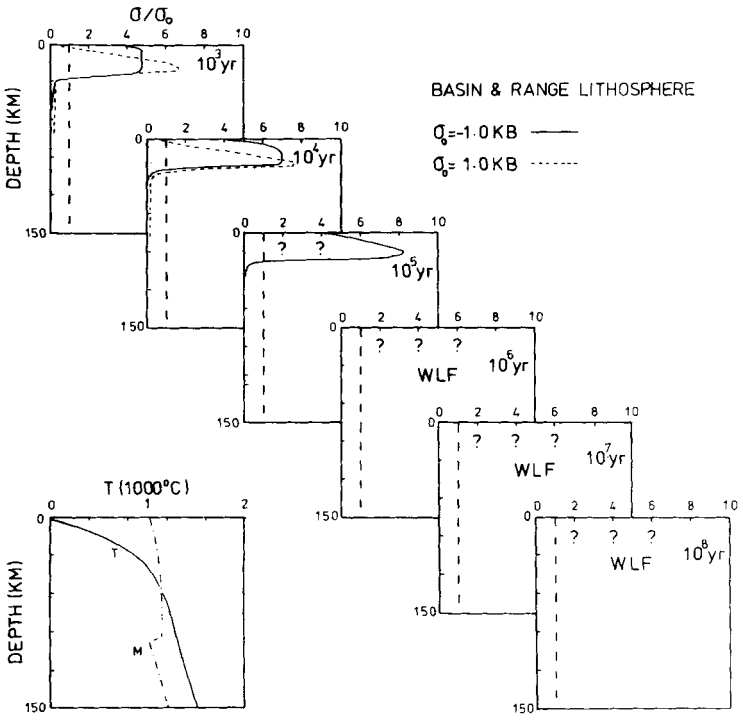

Figure 7. Stress in Basin and Range type lithosphere as a function of depth at various times after initial application of stress. $\sigma_0 = \pm 1.0$ kb.

gradient results in much lower viscosities in the middle and lower lithosphere than for ocean basin and continental lithosphere and consequently stress decay at depth and amplification in the upper lithosphere is much more rapid. Stress was initially applied over lithosphere 150 km thick to aid comparison with ordinary continental lithosphere.

For $\sigma_0 = \pm 0.1$ kb (Fig. 6) stress only remains in the upper ¼ of the lithosphere at 10^3 yr. The amplification factor is × 4. By 10^6 yr stress only remains in the upper $^1/_5$ of the lithosphere with an amplification factor of approximately × 6.5. At 10^8 yr the amplification factor has a value of × 7.5. The upper lithosphere stress amplification results in failure for σ_0 tensional (+ 0.1 kb) at 10^4 yr.

Fig. 7 shows stress behaviour for $\sigma_0 = \pm 1.0$ kb. Stress amplification results in failure for both compressive and tensional values of σ_0 – failure occurs earlier for tensional σ_0. The large amplification factors together with the extremely thin lithosphere thickness results, at about 10^4–10^5 yr, in complete or whole lithosphere failure (WLF). A situation develops where the upper lithosphere cannot sustain the amplified applied stress because of faulting, but its transfer to lower lithosphere, after faulting, results in its rapid transfer back to upper lithosphere levels because of lower lithosphere creep. Thus a cyclic process of upper lithosphere fracture and faulting will occur. For tensile applied stress, as occurs in the Basin and Range province, this would result in rapid crustal thinning.

6 Lithosphere stress response to internally derived stresses

Lateral density contrasts within the crust and/or mantle give rise to stress fields within the lithosphere. Examples of such internally derived stress fields are those found at passive con-

tinental margins (Bott & Dean 1972; Kusznir & Bott 1977), ocean ridges (Stephansson & Berner 1971), ocean trenches (Woodward 1976) and Basin and Range type regions (Bott & Kusznir 1979). In Fig. 8(a) a schematic diagram of lithosphere structure in a Basin and Range type region is shown. The area of plateau uplift is underlain by anomalous hot mantle which is lighter than laterally adjacent mantle and so provides isostatic compensation for the plateau uplift. The lateral density contrasts, shown in Fig. 8(c), result in a stress field which may be calculated using the finite element method (Zienkiewicz 1971). In Fig. 9(a) the deviatoric stresses arising from these lateral density contrasts are shown for an elastic

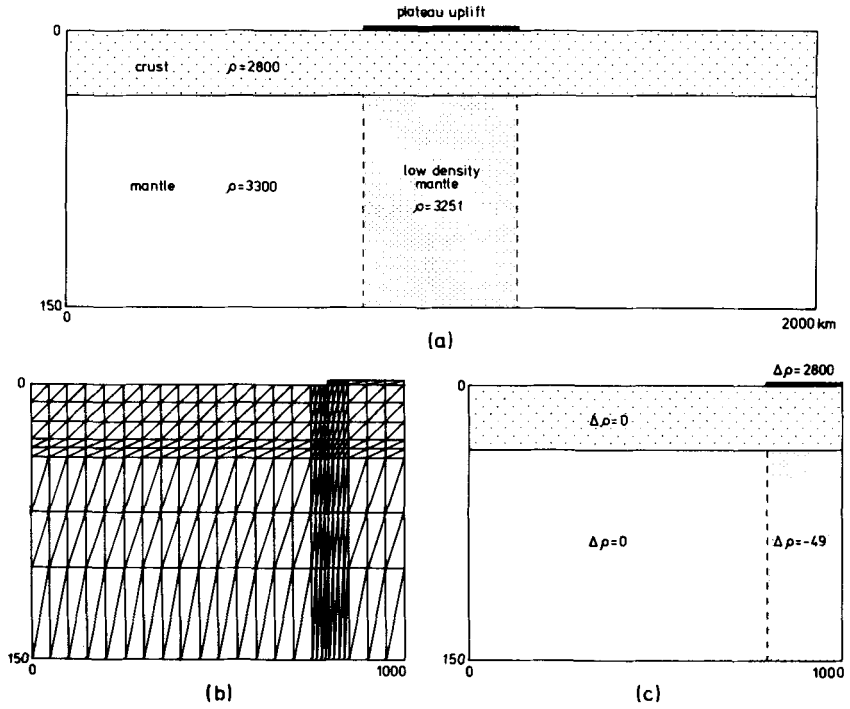

Figure 8. Schematic diagram of Basin and Range lithosphere structure showing: (a) lithosphere density distribution, (b) finite element subdivision of the lithosphere, (c) lateral density contrasts as used in the finite element calculation.

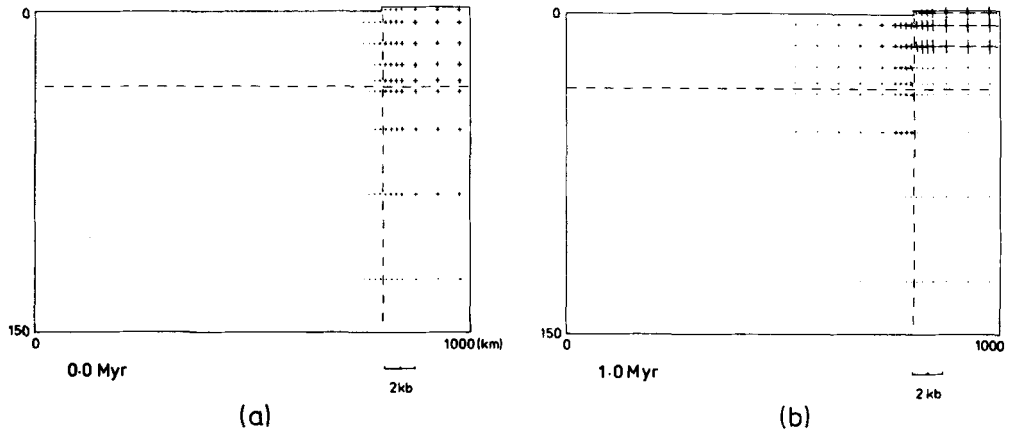

Figure 9. Deviatoric stresses within Basin and Range lithosphere due to lateral density contrasts. (a) Elastic solution. (b) Viscoelastic solution at 1 Myr.

lithosphere model. The region under the plateau uplift can be seen to be in relative horizontal tension. The finite element grid used for the calculation is shown in Fig. 8(b).

The stresses arising from lateral density contrasts have been calculated for a lithosphere with temperature- and stress-dependent viscoelastic properties. Apparent viscosity given by equation (2) has been used. The geotherms for a Basin and Range type region are shown in Fig. 6. This geotherm has been applied for the area under the plateau uplift while the adjacent continental lithosphere uses the geotherm shown in Fig. 4. A Young's modulus of 1.7×10^{11} Pa has been used for the lithosphere.

The stresses after 1 Myr of viscoelastic deformation are shown in Fig. 9(b). The stresses within the mantle under the platform uplift can be seen to have decayed while there is considerable amplification of the upper lithosphere stresses. The stress field at this time, for the viscoelastic model, is in approximate equilibrium. While the maximum deviatoric stress of the elastic model is about 0.3 kb, the maximum deviatoric stress of the viscoelastic model at 1 Myr is about 1.2 kb. This stress field at 1.0 Myr is sufficient to cause failure in the upper lithosphere.

7 Lithosphere stress response to bending stress

Bending or flexure of the lithosphere gives rise to stresses within the lithosphere. Such bending or flexure occurs at a plate boundary, in the case of subducting lithosphere, or in intraplate regions in response to sediment or volcanic loading. While the concave side of the lithosphere plate is put into horizontal compression, the convex side will be laterally extended and will suffer horizontal tension. In response to the bending stresses within the lithosphere, non-elastic deformation will occur resulting in the modification of the initial bending stress field. In the situation where the processes which initially bent the lithosphere maintain the lithosphere in a fixed bending geometry, viscoelastic deformation will result in the relaxation of the bending stresses. However, in the situation where the bending stresses and bending moments within the lithosphere are required to balance externally derived forces, such as load forces, the geometry of the bending lithosphere will not be constant and not all stresses may relax.

For the case where the bending geometry of the lithosphere remains constant the initial elastic bending stresses of the lithosphere may be regarded as initial stresses and the time-dependent relaxation of the stresses determined by the use of equations (11) and (12).

In Fig. 10 horizontal bending stress is shown as a function of time and depth. The instantaneous or elastic bending stresses are shown by the dashed diagonal line and have an arbitrary value of ± 1.0 kb at the top and bottom of the lithosphere respectively. Depth is shown as a fraction of lithosphere thickness. Stresses are shown for oceanic lithosphere – thickness 80 km, continental lithosphere – thickness 150 km and continental lithosphere with thickness 100 km. For all three models stress decays to zero at the bottom of the lithosphere. After 10^6 yr the stress at the top of the lithosphere has decreased to approximately half of its original value.

The depth of the neutral fibre can be seen to move progressively upwards with time. The effective lithosphere thickness at 1 Myr is approximately ½ of its initial value. Stress relaxation is greater for the initially thicker continental lithosphere. In all cases, however, an appreciable quantity of stress remains at 10^8 Myr.

8 Discussion

The coupled process of decay of stress in the lower lithosphere and associated amplification in the upper lithosphere has been shown to occur for both externally derived stress applied

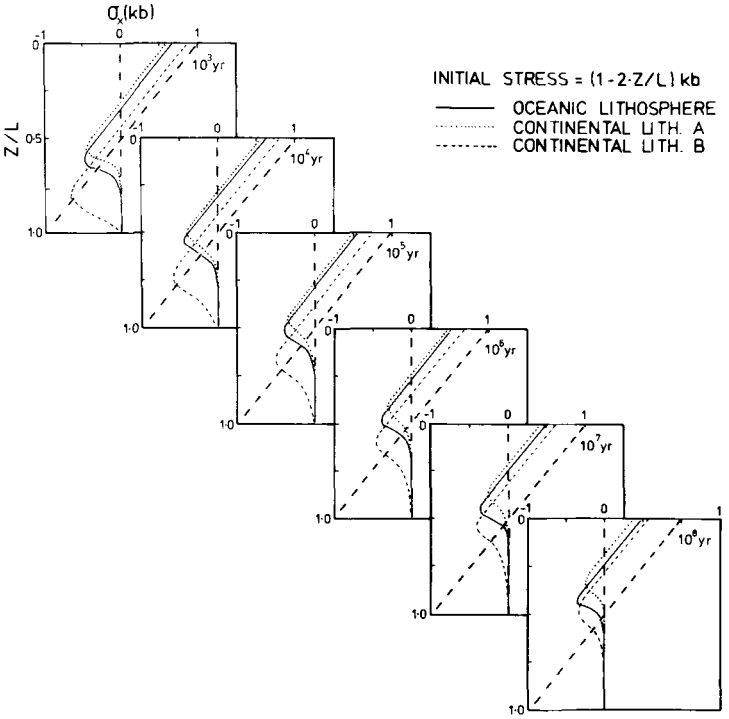

Figure 10. Stress generated by lithosphere bending for various lithosphere models, as a function of depth at various times after initial stress application.

to the lithosphere and stress derived internally by lateral density contrasts. This process provides a mechanism by which initially small stresses can be increased in the upper lithosphere to a magnitude where fracture, faulting and lithosphere deformation can take place. The rate and amount of stress amplification within the upper lithosphere is strongly controlled by the lithosphere geotherm. An applied stress of 1.0 kb applied to ocean basin or continental shield lithosphere results in stress amplification in the upper lithosphere of the order of $\times 2$ after a few million years. Some fracture of the upper lithosphere occurs for tensile applied stress; however, extensive lithosphere deformation does not occur. By 100 Myr a total lithosphere horizontal strain of the order of 0.1–0.01 per cent has taken place.

In the case, however, of lithosphere with a steeper geothermal gradient, for instance that of the Basin and Range province, the stress amplification in the upper lithosphere, in response to an applied stress of 1.0 kb, results in extensive fracture of the upper lithosphere. A cyclic process then occurs with transfer of stress by faulting from the upper lithosphere to the lower lithosphere, followed by rapid transfer of stress back to the upper lithosphere. Extensive lithosphere deformation in the form of either thrusting or lithosphere attenuation can result. For a stress of 1.0 kb applied to lithosphere with a Basin and Range geotherm, horizontal strains of 100 per cent or more per million years can occur.

A similar process also occurs for the density contrast derived stress field. In this case a localized high geothermal gradient can both generate the lithosphere density contrasts, and consequently the stress field, and provide the low values of apparent viscosity for rapid stress decay in the middle and lower lithosphere and the associated large stress amplification in the upper lithosphere.

The transfer of laterally applied stress from the lower to the upper lithosphere by lower

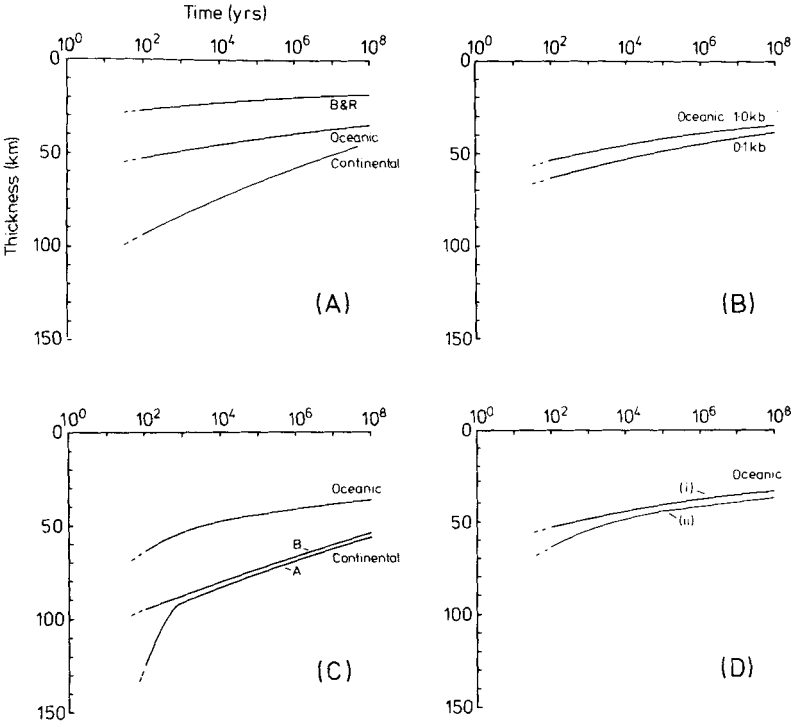

Figure 11. Effective lithosphere thickness as a function of time after initial stress application. (a) Effective lithosphere thicknesses compared for oceanic, continental and Basin and Range lithosphere for an applied stress of 1.0 kb. (b) Effective oceanic lithosphere thickness for an applied stress of 0.1 and 1.0 kb. (c) Effective lithosphere thickness, compared for oceanic and continental lithosphere models for stresses generated by bending. (d) Effective oceanic lithosphere thickness compared for applied stress model (i) and bending model (ii).

lithosphere creep, results in a decrease in the effective thickness of the lithosphere stress guide. The rate of stress decay in the lower lithosphere, and consequently the rate of decrease in the effective thickness of the lithosphere, is dependent on both the time after initial application of the stress and the geothermal gradient.

In Fig. 11(a) the decrease in the effective thickness of the lithosphere is shown as a function of time for oceanic, continental and Basin and Range type lithosphere. The effective thickness of the lithosphere is here defined as the depth to the point at which the stress field falls to $\sigma_{max}/2$. The lithosphere thickness refers to a model with an applied stress of 1.0 kb. At 1 Myr after the application of stress the lithosphere thicknesses are approximately 20 km for the Basin and Range lithosphere, 40 km for oceanic lithosphere and 60 km for continental lithosphere.

Effective lithosphere thickness depends on the magnitude of the applied stress. In Fig. 11(b) the effective lithosphere thickness is shown for oceanic lithosphere with applied stresses of 0.1 and 1.0 kb. Because effective viscosity decreases with increase in the level of the applied stress; the stress decays more rapidly in the lower lithosphere for higher levels of applied stress. Consequently the effective lithosphere thickness is less for an applied stress of 1.0 kb.

The effective thickness of lithosphere for bending stresses arising from a constant bending geometry (Section 7) also decreases with time and is shown in Fig. 11(c). Effective lithosphere thickness is defined as twice the depth of the neutral fibre. The thicknesses shown in Fig.

11(c) are for a model with maximum initial bending stresses of ± 1.0 kb. The thickness of the oceanic lithosphere at 1 Myr is about 43 km. Thicknesses of continental lithosphere are shown for two continental lithosphere models. Continental lithosphere model A is initially 150 km thick while model B is 100 km thick. At 1 Myr both models have a thickness of the order of 65 km with model A (initially 150 km thick) having the slightly thicker value.

In Fig. 11(d) oceanic lithosphere effective thicknesses are compared for the laterally applied stress model (curve i) and the bending model (curve ii). The thicknesses are generally similar; however, the laterally applied stress model has the slightly smaller values.

Watts *et al.* (1980) have summarized oceanic lithosphere thickness estimates using both seamount and trench outer-rise flexure estimates. They show that the thickness of lithosphere based on flexure is controlled by the age of the lithosphere at the time of loading, not by the age of the load. Watts & Cochran (1974) found that, for thermally equilibrated ocean basin lithosphere, the flexural rigidity associated with the Hawaiian Emperor seamount chain was similar for loads of 3 and 70 Myr age. The curves of Fig. 11(d) are consistent with this observation and predict very little change in lithosphere thickness between 1 and 100 Myr after initial stress application. The lithosphere model presented in this paper suggests that the major stress transfer from the lower to the upper lithosphere and associated thinning of the lithosphere takes place over a period of substantially less than 1 Myr. Consequently the flexural rigidity parameter can be assumed to undergo the majority of its decrease within a similar time period.

For thermally equilibrated ocean basin with age greater than 80 Myr the values of lithosphere thickness, using the compilation of Watts *et al.*, lie predominantly between 20 and 30 km with an average value of the order of 25 km. The lithosphere thickness estimates presented in Fig. 11 are generally overestimates of effective lithosphere thickness since fracture of the upper lithosphere, resulting as a consequence of stress amplification, will further reduce the thickness (see Figs 3, 5, 6 and 7). The effective thicknesses of the oceanic lithosphere model without fracture show long term values of approximately 35 km. From Fig. 3 it can be seen that, depending on the sign of the applied stress and its amplitude, model lithosphere thicknesses can be reduced by approximately 5 km to a thickness of the order of 30 km; a value more comparable with the observations of Watts *et al.* The values of lithosphere thickness are not directly comparable, however, since the stress field associated with the observed flexure is generated by loading while the model stress field relates either to an applied, externally derived stress or to constant geometry bending. Coble creep (diffusion creep), which may take place at lower temperatures than dislocation creep, or a Dorn law rheology may additionally reduce the effective lithosphere thickness of the model.

References

Bott, M. H. P. & Dean, D. S., 1972. Stress systems at young continental margins, *Nature (Phys. Sci.)*, **235**, 23–25.

Bott, M. H. P. & Kusznir, N. J., 1979. Stress distributions associated with compensated plateau uplift structures with application to the continental splitting mechanism, *Geophys. J. R. astr. Soc.*, **56**, 451–459.

Brace, W. F., 1961. Dependence of fracture strength on grain size, *Bull. Miner. Inds Exp. Stn Penn. St. Univ.*, **76**, 99–103.

Cathles, L. M., 1975. *The Viscosity of the Earth's Mantle*, Princeton University Press, 386 pp.

Cazenave, A., Lago, B., Dominh, K. & Lambeck, K., 1980. On the response of the ocean lithosphere to sea-mount loads from *Geos 3* satellite radar-altimeter observations, *Geophys. J. R. astr. Soc.*, **63**, 233–252.

Forsyth, D. W., 1975. The early structural evolution and anisotropy of the oceanic upper mantle, *Geophys. J. R. astr. Soc.*, **43**, 103–162.

Forsyth, D. W., 1977. The evolution of the upper mantle beneath mid-ocean ridges, *Tectonophys.*, **38**, 89–118.

Froidevaux, C. & Schubert, G., 1975. Plate motion and structure of the continental asthenosphere: a realistic model of the upper mantle, *J. geophys. Res.*, **80**, 2553–2564.

Goetze, C., 1978. The mechanism of creep in olivine, *Phil. Trans. R. Soc. A*, **288**, 99–119.

Green, D. H., 1973. Experimental melting studies on a model upper mantle composition at high pressure under water-saturated and water-undersaturated conditions. *Earth planet. Sci. Lett.*, **19**, 37–53.

Haigh, B. I. R., 1973. North Atlantic oceanic topography and lateral variations in the upper mantle, *Geophys. J. R. astr. Soc.*, **33**, 405–420.

Haskell, N. A., 1937. The viscosity of the asthenosphere, *Am. J. Sci.*, **33**, 22–28.

Herrin, E., 1972. A comparative study of upper mantle models: Canadian shield and Basin and Range provinces, in *The Nature of the Solid Earth*, pp. 216–231, ed. Robertson, E. C., McGraw-Hill, New York.

Kohlstedt, D. L. & Geotze, C., 1974. Low-stress high-temperature creep in olivine single crystals, *J. geophys. Res.*, **79**, 2045–2051.

Kusznir, N. J. & Bott, M. H. P., 1977. Stress concentration in the upper lithosphere caused by underlying viscoelastic creep, *Tectonophys.*, **43**, 247–256.

Lago, B. & Cazenave, A., 1981. State of stress in the oceanic lithosphere in response to loading, *Geophys. J. R. astr. Soc.*, **64**, 785–800.

Mercier, J. C. & Carter, N. L., 1975. Pyroxene geotherms, *J. geophys. Res.*, **80**, 3349–3362.

Murrell, S. A. F., 1958. *Mechanical Properties of Non-metallic Brittle Materials*, pp. 123–145, ed. Walton, W. H., Butterworths, London.

Murrell, S. A. F., 1976. Rheology of the lithosphere – experimental indications, *Tectonophys.*, **36**, 5–24.

Neugebauer, H. J. & Breitmayer, G., 1975. Dominant creep mechanism and the descending lithosphere, *Geophys. J. R. astr. Soc.*, **43**, 873–895.

Schubert, G., Froidevaux, C. & Yuen, D. A., 1976. Oceanic lithosphere and asthenosphere: thermal and mechanical structure, *J. geophys. Res.*, **81**, 3525–3540.

Sclater, J. G. & Francheteau, J., 1970. The implications of terrestrial heat flow observations on current tectonic and geochemical models of the crust and upper mantle of the earth, *Geophys. J. R. astr. Soc.*, **20**, 509–542.

Stephansson, O. & Berner, H., 1971. The finite element method in tectonic processes, *Phys. Earth planet. Int.*, **4**, 301–321.

Turcotte, D. L. & Oxburgh, E. R., 1976. Stress accumulation in the lithosphere, *Tectonophys*, **35**, 183–199.

Walcott, R. I., 1970. Flexural rigidity, thickness and viscosity of the lithosphere, *J. geophys. Res.*, **75**, 3941–3954.

Watts, A. B., Bodine, J. H. & Steckler, M. S., 1980. Observations of flexure and the state of stress in the oceanic lithosphere, *J. geophys. Res.*, **85**, 6369–6376.

Watts, A. B. & Cochran, J. R., 1974. Gravity anomalies and flexure of the lithosphere along the Hawaiian-Emperor Seamount Chain, *Geophys. J. R. astr. Soc.*, **38**, 119–141.

Watts, A. B., Cochran, J. R. & Selzer, G., 1975. Gravity anomalies and flexure of the lithosphere: a three-dimensional study of the Great Meteor seamount, Northeast Atlantic, *J. geophys. Res.*, **80**, 1391–1398.

Woodward, D. J., 1976. Visco-elastic finite element analysis of subduction zones, *unpublished PhD thesis*, University of Durham.

Zienkiewicz, O. C., 1971. *The Finite Element Method in Engineering Science*, McGraw-Hill, London, 521 pp.